
Deep Predictive Coding Networks

Rakesh Chalasani **Jose C. Principe**
Department of Electrical and Computer Engineering
University of Florida, Gainesville, FL 32611
rakeshch@ufl.edu, principe@cnel.ufl.edu

Abstract

The quality of data representation in deep learning methods is directly related to the prior model imposed on the representations; however, generally used fixed priors are not capable of adjusting to the context in the data. To address this issue, we propose deep predictive coding networks, a hierarchical generative model that empirically alters priors on the latent representations in a dynamic and context-sensitive manner. This model captures the temporal dependencies in time-varying signals and uses top-down information to modulate the representation in lower layers. The centerpiece of our model is a novel procedure to infer sparse states of a dynamic model which is used for feature extraction. We also extend this feature extraction block to introduce a pooling function that captures locally invariant representations. When applied on a natural video data, we show that our method is able to learn high-level visual features. We also demonstrate the role of the top-down connections by showing the robustness of the proposed model to structured noise.

1 Introduction

The performance of machine learning algorithms is dependent on how the data is represented. In most methods, the quality of a data representation is itself dependent on prior knowledge imposed on the representation. Such prior knowledge can be imposed using domain specific information, as in SIFT [1], HOG [2], etc., or in learning representations using fixed priors like sparsity [3], temporal coherence [4], etc. The use of fixed priors became particularly popular while training deep networks [5–8]. In spite of the success of these general purpose priors, they are not capable of adjusting to the context in the data. On the other hand, there are several advantages to having a model that can “actively” adapt to the context in the data. One way of achieving this is to *empirically alter the priors* in a dynamic and context-sensitive manner. This will be the main focus of this work, with emphasis on visual perception.

Here we propose a predictive coding framework, where a *deep locally-connected* generative model uses “top-down” information to empirically alter the priors used in the lower layers to perform “bottom-up” inference. The centerpiece of the proposed model is extracting sparse features from time-varying observations using a *linear dynamical model*. To this end, we propose a novel procedure to infer *sparse states* (or features) of a dynamical system. We then extend this feature extraction block to introduce a pooling strategy to learn invariant feature representations from the data. In line with other “deep learning” methods, we use these basic building blocks to construct a hierarchical model using greedy layer-wise unsupervised learning. The hierarchical model is built such that the output from one layer acts as an input to the layer above. In other words, the layers are arranged in a Markov chain such that the states at any layer are only dependent on the representations in the layer below and above, and are independent of the rest of the model. The overall goal of the dynamical system at any layer is to make the best *prediction* of the representation in the layer below using the top-down information from the layers above and the temporal information from the previous states. Hence, the name *deep predictive coding networks* (DPCN).

1.1 Related Work

The DPCN proposed here is closely related to models proposed in [9, 10], where predictive coding is used as a statistical model to explain cortical functions in the mammalian brain. Similar to the proposed model, they construct hierarchical generative models that seek to infer the underlying causes of the sensory inputs. While Rao and Ballard [9] use an update rule similar to Kalman filter for inference, Friston [10] proposed a general framework considering all the higher-order moments in a continuous time dynamic model. However, neither of the models is capable of extracting discriminative information, namely a sparse and invariant representation, from an image sequence that is helpful for high-level tasks like object recognition. Unlike these models, here we propose an efficient inference procedure to extract locally invariant representation from image sequences and progressively extract more abstract information at higher levels in the model.

Other deep learning methods, like Deep Belief Networks (DBN) [11], auto-encoders [8, 12] and predictive sparse decomposition [13], are also related to the model proposed here. All these models are constructed on similar underlying principles: (1) like ours, they also use greedy layer-wise unsupervised learning to construct a hierarchical model and (2) each layer consists of an encoder and a decoder. The key to these models is to learn both encoding and decoding concurrently (with some regularization like sparsity [13], denoising [8] or weight sharing [11]), while building the deep network as a feed forward model using only the encoder. The idea is to approximate the latent representation using only the feed-forward encoder, while avoiding the decoder which typically requires a more expensive inference procedure. However in DPCN there is no encoder. Instead, DPCN relies on an efficient inference procedure to get a more accurate latent representation. As we will show below, the use of reciprocal top-down and bottom-up connections make the proposed model more robust to structured noise during recognition and also allows it to perform low-level tasks like image denoising.

To scale to large images, several convolutional models are also proposed in a similar deep learning paradigm [5–7]. Inference in these models is applied over an entire image, rather than small parts of the input. DPCN can also be extended to form a convolutional network, but this will not be discussed here.

2 Model

In this section, we begin with a brief description of the general predictive coding framework and proceed to discuss the details of the architecture used in this work. The basic block of the proposed model that is pervasive across all layers is a generalized state-space model:

$$\begin{aligned}\tilde{\mathbf{y}}_t &= \mathcal{F}(\mathbf{x}_t, \mathbf{u}_t) + \mathbf{n}_t \\ \mathbf{x}_t &= \mathcal{G}(\mathbf{x}_{t-1}, \mathbf{u}_t) + \mathbf{v}_t\end{aligned}\tag{1}$$

where $\tilde{\mathbf{y}}_t \in \mathbb{R}^P$ is the data and \mathcal{F} and \mathcal{G} are some functions that can be parameterized, say by θ . The terms $\mathbf{u}_t \in \mathbb{R}^D$ are called the *unknown causes*. Since we are usually interested in obtaining abstract information from the observations, the causes are encouraged to have a non-linear relationship with the observations. The hidden states, $\mathbf{x}_t \in \mathbb{R}^K$, then “mediate the influence of the cause on the output and endow the system with memory” [10]. The terms \mathbf{v}_t and \mathbf{n}_t are stochastic and model uncertainty. Several state-space models can now be stacked, such that the output from one acts as an input to the layer above, to form a hierarchical model. The inputs and the states of the l th layer are of the form:

$$\begin{aligned}\mathbf{u}_t^{(l-1)} &= \mathcal{F}(\mathbf{x}_t^{(l)}, \mathbf{u}_t^{(l)}) + \mathbf{n}_t^{(l)} \\ \mathbf{x}_t^{(l)} &= \mathcal{G}(\mathbf{x}_{t-1}^{(l)}, \mathbf{u}_t^{(l)}) + \mathbf{v}_t^{(l)}\end{aligned}\tag{2}$$

where $l \in \{1, 2, \dots, L\}$ ¹. This model describes an L -layered network at any time ‘ t ’. The terms $\mathbf{v}_t^{(l)}$ and $\mathbf{n}_t^{(l)}$ form stochastic fluctuations at the higher layers and enter each layer independently. In other words, this model forms a Markov chain across the layers, simplifying the inference procedure. Notice how the causes at the lower layer form the “observations” to the layer above — the causes form the link between the layers, and the states link the dynamics over time. The important point in

¹When $l = 1$, i.e., at the bottom layer, $\mathbf{u}_t^{(l-1)} = \mathbf{y}_t$, where \mathbf{y}_t the input data.

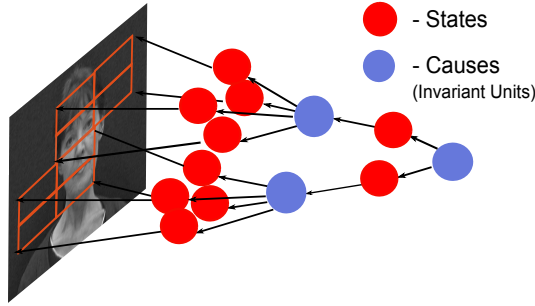


Figure 1: Shows the distributive hierarchical model used in this work. Refer to text for more details.

this design is that the higher-level predictions influence the lower levels' inference. The predictions from a higher layer non-linearly enter into the state space model by empirically altering the prior on the causes. In summary, the top-down connections and the temporal dependencies in the state space influence the latent representation at any layer.

2.1 Architecture

In this work, an architecture and a form of the functions \mathcal{F} and \mathcal{G} in (1) are proposed such that they are more pertinent to capture abstract information from video data. To this end, a distributive architecture (see Figure 1) is used, where several parts of a video frame are encoded in parallel and are combined together in the higher layers. Here each frame is divided into over-lapping patches and are used as observations at the bottom layer. From a small group of contiguous patches (in the image domain) relevant features (states) are *extracted* and *pooled* together to form a locally invariant representation (causes), all while considering the top-down predictions. In the layer above, a similar procedure is used to combine the causes from the bottom layer and so on.

As discussed in section 1, the feature extraction part involves inferring sparse states of a linear dynamical model with observation matrix $\mathbf{C} \in \mathbb{R}^{P \times K}$ and state-transition matrix $\mathbf{A} \in \mathbb{R}^{K \times K}$. The pooling function, parameterized by $\mathbf{B} \in \mathbb{R}^{K \times D}$, is learned from the data (discussed in section 2.2). So, let $\theta = \{\mathbf{A}, \mathbf{B}, \mathbf{C}\}$ be the set of parameters that describe \mathcal{F} and \mathcal{G} in (1). In the following sections each of these parts will be explained in more detail.

2.2 Energy Function

To begin with, we consider a single layered network, where $\tilde{\mathbf{y}}_t$ is a small patch in the input frame at any time t . As described in the architecture above, each layer consists of two distinctive processing parts: feature extraction (inferring states) and pooling (inferring causes). For the first part, sparse coding is used in conjunction with a linear state space model to map the inputs onto an over-complete dictionary of filters \mathbf{C} , and to keep track of the dynamics in the latent states \mathbf{x}_t using the state-transition matrix \mathbf{A} . More formally, inference of the features \mathbf{x}_t is performed by finding a representation that minimizes the energy function:

$$E_1(\mathbf{x}_t, \tilde{\mathbf{y}}_t, \mathbf{C}, \mathbf{A}) = \|\tilde{\mathbf{y}}_t - \mathbf{C}\mathbf{x}_t\|_2^2 + \lambda\|\mathbf{x}_t - \mathbf{A}\mathbf{x}_{t-1}\|_1 + \gamma\|\mathbf{x}_t\|_1 \quad (3)$$

Notice that the second term involving the state-transition is also constrained to be sparse to make the state-space representation consistent.

On the other hand, the causes \mathbf{u}_t are inferred such that a small group of features (or states), \mathbf{x}_t , are pooled together to extract a representation that is invariant to common transformations within a spatial neighborhood. In line with [14], this pooling function is also learned such that it can capture the dependencies between the features. The causes \mathbf{u}_t are inferred using the accumulated states by minimizing the energy function:

$$E_2(\mathbf{u}_t, \mathbf{x}_t, \mathbf{B}) = \sum_{n=1}^N \left(\sum_{k=1}^K |\gamma_k \cdot x_{t,k}^{(n)}| \right) + \beta\|\mathbf{u}_t\|_1 \quad (4)$$

$$\gamma_k = \gamma_0 \left[\frac{1 + \exp(-[\mathbf{B}\mathbf{u}_t]_k)}{2} \right]$$

where $n \in \{1, 2, \dots, N\}$ represents a set of contiguous blocks (w.r.t. the position in the image space) that are ‘‘pooled’’ together and $\gamma_0 > 0$ is some constant.

Building a Hierarchy: The architecture described above is capable of extracting features from a small part of the inputs. Using this basic building block, it is easy to construct a hierarchy by treating the causes from the layer $(l - 1)$, $\mathbf{u}_t^{(l-1)}$, as inputs for layer (l) . With this, a single combined cost function E_l for layer l can be written as:

$$E_l(\mathbf{x}_t^{(l)}, \mathbf{u}_t^{(l)}, \boldsymbol{\theta}^{(l)}) = \sum_{n=1}^N \left(\frac{1}{2} \|\mathbf{u}_t^{(l-1,n)} - \mathbf{C}^{(l)} \mathbf{x}_t^{(l,n)}\|_2^2 + \lambda \|\mathbf{x}_t^{(l,n)} - \mathbf{A}^{(l)} \mathbf{x}_{t-1}^{(l,n)}\|_1 \right. \\ \left. + \sum_{k=1}^K |\gamma_{t,k}^{(l)} \cdot x_{t,k}^{(l,n)}| \right) + \beta \|\mathbf{u}_t^{(l)}\|_1 + \frac{1}{2} \|\mathbf{u}_t^{(l)} - \hat{\mathbf{u}}_t^{(l+1)}\|_2^2 \quad (5)$$

$$\gamma_{t,k}^{(l)} = \gamma_0 \left[\frac{1 + \exp(-[\mathbf{B}^{(l)} \mathbf{u}_t^{(l)}]_k)}{2} \right]$$

where $\boldsymbol{\theta}^{(l)} = \{\mathbf{A}^{(l)}, \mathbf{B}^{(l)}, \mathbf{C}^{(l)}\}$. Notice the additional term involving $\hat{\mathbf{u}}_t^{(l+1)}$. This comes from the top-down information, where $\hat{\mathbf{u}}_t^{(l+1)}$ is the prediction of the causes for layer (l) using the states in layer $(l + 1)$. The *combined prior* now imposed on the causes, $\beta \|\mathbf{u}_t^{(l)}\|_1 + \frac{1}{2} \|\mathbf{u}_t^{(l)} - \hat{\mathbf{u}}_t^{(l+1)}\|_2^2$, is similar to the elastic net prior discussed in [15], leading to a smoother and biased estimate of the causes. More discussion about this below.

2.3 Learning

As discussed, we greedily build the hierarchy, training each layer at a time without considering any top-down information. So, to learn the parameters for layer (l) , we alternatively minimize $E_l(\mathbf{x}_t^{(l)}, \mathbf{u}_t^{(l)}, \boldsymbol{\theta}^{(l)})$ without the top-down prediction ($\hat{\mathbf{u}}_t^{(l+1)} = \mathbf{0}$). We first minimize E_l over the states and the causes with the parameters fixed (inference), and then fix the inferred states and causes to minimize E_l over the parameters. In the following sections, we describe each of these procedures in more detail.

Notation: To make things less cumbersome, henceforth, unless specified, the superscript (l) indicating the layer is considered implicit. Also, we use $\mathbf{y}_t^{(n)}$ (with (l) being left implicit) in place of $\mathbf{u}_t^{(l-1,n)}$ to describe the inputs to the l th layer.

2.3.1 Inference

In this section, keeping aside the causes, we first focus on inferring sparse states in a linear dynamical model that can represent an input sequence. Then we discuss joint inference of both the states and the causes that minimizes the energy function in (5).

Inferring States: Inferring sparse states, given the parameters, from a linear dynamical system forms the crux of our model. This is performed by finding the solution that minimizes the energy function E_1 in (3) with respect to the states \mathbf{x}_t . It is easy to show that this is equivalent to finding the mode of the distribution $p(\mathbf{x}_t | \mathbf{y}_t, \mathbf{x}_{t-1})$. Here there are two priors of the states: the temporal dependence and the sparsity term. Although this energy function E_1 is convex in \mathbf{x}_t , the presence of two non-smooth terms makes it hard to use standard optimization techniques used for sparse coding alone. A similar problem is solved using dynamic programming [16], homotopy [17] and Bayesian sparse coding [18]; however, the optimization used in these models is computationally expensive for use in large scale problems like object recognition.

To overcome this, inspired by the method proposed in [19] for structured sparsity, we propose an approximate solution that is consistent and able to use efficient solvers like fast iterative shrinkage thresholding algorithm (FISTA) [20]. The key to our approach is to first use Nesterov’s smoothness method [19, 21] to approximate the non-smooth state transition term. The resulting energy function is a convex and continuously differentiable function in \mathbf{x}_t with a sparsity constraint, and hence, can be efficiently solved using proximal methods like FISTA.

To begin, let $\Omega(\mathbf{x}_t) = \|\mathbf{e}_t\|_1$ where $\mathbf{e}_t = (\mathbf{x}_t - \mathbf{A}\mathbf{x}_{t-1})$. The idea is to find a smooth approximation to this function $\Omega(\mathbf{x}_t)$ in \mathbf{e}_t . Notice that, since \mathbf{e}_t is a linear function on \mathbf{x}_t , the approximation will also be smooth w.r.t. \mathbf{x}_t . Now, we can re-write $\Omega(\mathbf{x}_t)$ using the dual norm of ℓ_1 as

$$\Omega(\mathbf{x}_t) = \arg \max_{\|\alpha\|_\infty \leq 1} \alpha^T \mathbf{e}_t$$

where $\alpha \in \mathbb{R}^k$. Using the smoothing approximation from Nesterov [21] on $\Omega(\mathbf{x}_t)$:

$$\Omega(\mathbf{x}_t) \approx f_\mu(\mathbf{e}_t) = \arg \max_{\|\alpha\|_\infty \leq 1} [\alpha^T \mathbf{e}_t - \mu d(\alpha)] \quad (6)$$

where $d(\cdot) = \frac{1}{2}\|\alpha\|_2^2$ is a smoothing function and μ is a smoothness parameter. From Nesterov's theorem [21], it can be shown that $f_\mu(\mathbf{e}_t)$ is convex and continuously differentiable in \mathbf{e}_t and the gradient of $f_\mu(\mathbf{e}_t)$ with respect to \mathbf{e}_t takes the form

$$\nabla_{\mathbf{e}_t} f_\mu(\mathbf{e}_t) = \alpha^* \quad (7)$$

where α^* is the optimal solution to $f_\mu(\mathbf{e}_t) = \arg \max_{\|\alpha\|_\infty \leq 1} [\alpha^T \mathbf{e}_t - \mu d(\alpha)]$. This implies, by using the chain rule, that $f_\mu(\mathbf{e}_t)$ is also convex and continuously differentiable in \mathbf{x}_t and with the same gradient.

With this smoothing approximation, the overall cost function from (3) can now be re-written as

$$\mathbf{x}_t = \arg \min_{\mathbf{x}_t} \frac{1}{2} \|\mathbf{y}_t - \mathbf{C}\mathbf{x}_t\|_2^2 + \lambda f_\mu(\mathbf{e}_t) + \gamma \|\mathbf{x}_t\|_1 \quad (8)$$

with the smooth part $h(\mathbf{x}_t) = \frac{1}{2} \|\mathbf{y}_t - \mathbf{C}\mathbf{x}_t\|_2^2 + \lambda f_\mu(\mathbf{e}_t)$ whose gradient with respect to \mathbf{x}_t is given by

$$\nabla_{\mathbf{x}_t} h(\mathbf{x}_t) = \mathbf{C}^T(\mathbf{y}_t - \mathbf{C}\mathbf{x}_t) + \lambda \alpha^* \quad (9)$$

Using the gradient information in (9), we solve for \mathbf{x}_t from (8) using FISTA [20].

Inferring Causes: As discussed in section 2.2, the causes are inferred such that they can capture dependencies (or high-order statistical regularities) in the features \mathbf{x}_t . They are inferred by minimizing E_2 with respect to \mathbf{u}_t , where we define a generative model that modulates the sparsity of the accumulated state vector, $\sum_n \|\mathbf{x}^{(n)}\|_1$. Note that, similar to traditional hard-wired pooling operations like *max* or *average* pooling, accumulating the states (adding the absolute valued states from a local neighborhood) only leads to translation invariance. However, by modeling the higher-order statistics one may disentangle more complex local transformations like rotation, position, etc., from the data. Karklin and Lewicki [14] proposed a generative model to learn these relationships between the filters in a generalized ICA using two separate training modules. Here we extend this model to include both local pooling as well as learning local transformations, while jointly inferring the causes along with the states.

Firstly, we discuss inferring the causes \mathbf{u}_t given the states \mathbf{x}_t by minimizing E_2 in (5) with respect to \mathbf{u}_t . Here we observe that FISTA can be readily applied to infer \mathbf{u}_t , as the smooth part of the function E_2 , given by:

$$h(\mathbf{u}_t) = \sum_{k=1}^K \left(\gamma_0 \left[\frac{1 + \exp(-[\mathbf{B}\mathbf{u}_t]_k)}{2} \right] \cdot \sum_{n=1}^N |x_{t,k}^{(n)}| \right) + \frac{1}{2} \|\mathbf{u}_t\|^2 \quad (10)$$

is convex, continuously differentiable and Lipschitz in \mathbf{u}_t [22]³. Following [20], it is easy to obtain a bound on the convergence rate of the solution.

Joint Inference: We showed thus far that both \mathbf{x}_t and \mathbf{u}_t can be inferred from their respective energy functions using a first-order proximal method called FISTA. However, for joint inference we have to minimize the combined function in (5) over both \mathbf{x}_t and \mathbf{u}_t . We do this by alternately updating \mathbf{x}_t and \mathbf{u}_t while holding the other fixed and using a *single* FISTA update step at each iteration. It is important to point out that the internal FISTA step size parameters are maintained between iterations. This procedure is equivalent to alternating minimization using gradient descent. Although this procedure no longer guarantees convergence of both \mathbf{x}_t and \mathbf{u}_t to the optimal solution, in all of our simulations it lead to a reasonably good solution.

²Please refer to the supplementary material for the exact form of α^* .

³The matrix \mathbf{B} is initialized with non-negative entries and continues to be non-negative without any additional constraints [22]. Also, notice that the presence of the top-down prediction term $\mathbf{u}_t^{(l+1)}$ does not change the procedure described here.

2.3.2 Parameter Updates

With \mathbf{x}_t and \mathbf{u}_t fixed, we update the parameters by minimizing E_l in (5) with respect to $\boldsymbol{\theta}$. Since the inputs here are a time-varying sequence, the parameters are updated using dual estimation filtering [23]; i.e., we put an additional constraint on the parameters such that they follow a state space equation of the form:

$$\boldsymbol{\theta}_t = \boldsymbol{\theta}_{t-1} + \mathbf{z}_t \quad (11)$$

This keeps track of their temporal relationships. Along with this constraint, we update the parameters using gradient descent. Notice that with a fixed \mathbf{x}_t and \mathbf{u}_t , each of the parameter matrices can be updated independently. Matrices \mathbf{C} and \mathbf{B} are column normalized after the update to avoid any trivial solution.

Mini-Batch Update: To get faster convergence, the parameters are updated after performing inference over a large sequence of inputs instead of at every time instance. With this ‘‘batch’’ of signals, more sophisticated gradient methods, like conjugate gradient, can be used and, hence, can lead to more accurate and faster convergence.

2.4 Inference with top-down information

The above learning procedure allows us to train a hierarchical model with a layer-wise learning procedure. As discussed above, this model is constructed such that the layers are arranged in a Markov chain, i.e., each block at any layer is only influenced by the causes in the layer below and the layer above. Ideally, to perform inference across all the layers, all the states and the causes have to be updated simultaneously depending on the present state of all the other layers until the model reaches equilibrium. However, such a procedure can be very slow in practice. Instead, we propose to perform only a single top-down flow of information and then a single bottom-up inference using this top-down information.

For the top-down information flow, at any layer (l) we propagate the most likely causes. The prediction of the causes at any time t at layer (l) uses the previous state, $\mathbf{x}_{t-1}^{(l)}$ at layer l and the causes $\hat{\mathbf{u}}_t^{(l+1)}$. More formally, the top-down prediction at layer l is obtained as

$$\begin{aligned} \hat{\mathbf{x}}_t^{(l)} &= \arg \min_{\mathbf{x}_t^{(l)}} \lambda^{(l)} \|\mathbf{x}_t^{(l)} - \mathbf{A}^{(l)} \mathbf{x}_{t-1}^{(l)}\|_1 + \gamma_0 \sum_{k=1}^K |\hat{\gamma}_{t,k} \cdot \mathbf{x}_{t,k}^{(l)}| \quad (12) \\ \text{where } \hat{\gamma}_{t,k} &= (1 + \exp(-[\mathbf{B}\hat{\mathbf{u}}_t^{(l+1)}]_k))/2 \\ \hat{\mathbf{u}}_t^{(l)} &= \mathbf{C}^{(l)} \hat{\mathbf{x}}_t^{(l)} \end{aligned}$$

At the top most layer, L , a ‘‘bias’’ is set such that $\hat{\mathbf{u}}_t^{(L)} = \hat{\mathbf{u}}_{t-1}^{(L)}$, i.e., the top-layer induces some temporal coherence on the final outputs. From (12), it is easy to show that the predicted states for layer l can be obtained as

$$\hat{x}_{t,k}^{(l)} = \begin{cases} [\mathbf{A}^{(l)} \mathbf{x}_{t-1}^{(l)}]_k, & \gamma_0 \gamma_{t,k} < \lambda^{(l)} \\ 0, & \gamma_0 \gamma_{t,k} \geq \lambda^{(l)} \end{cases} \quad (13)$$

Following this, the predicted causes $\hat{\mathbf{u}}_t^{(l)}$, $\forall l \in \{1, 2, \dots, L\}$ are substituted back in (5) and a layer-wise bottom-up inference is performed as described in section 2.3.

3 Experiments

3.1 Receptive fields of causes in the hierarchical model

Firstly, we would like to test the ability of the proposed model to learn complex features in the higher-layers of the model. For this we train a two layered network from a natural video. Each frame in the video was first contrast normalized as described in [13]. Then, we train the first layer of the model on 4 overlapping contiguous 15×15 pixel patches from this video; this layer has 400 dimensional states and 100 dimensional causes. The causes pool the states related to all the

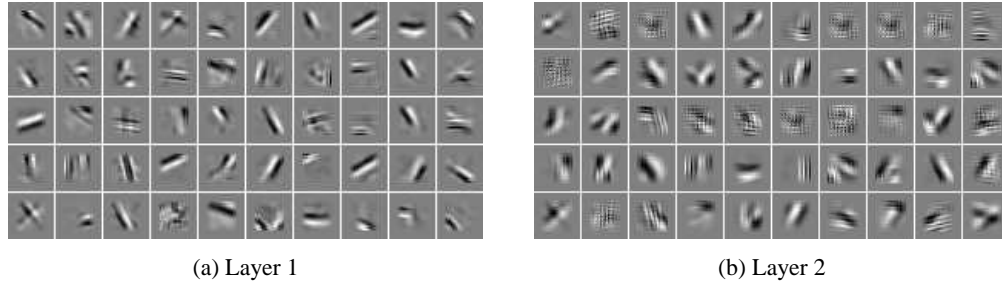


Figure 2: Shows the receptive fields of (a) layer 1 causes and (b) layer 2 causes from natural videos. The receptive fields are constructed as a weighted combination of the primitive filters at the bottom layer.

4 patches. The separation between the overlapping patches here was 2 pixels, implying that the receptive field of the causes in the first layer is 17×17 pixels. Similarly, the second layer is trained on 4 causes from the first layer obtained from 4 overlapping 17×17 pixel patches from the video. The separation between the patches here is 3 pixels, implying that the receptive field of the causes in the second layer is 20×20 pixels. The second layer contains 200 dimensional states and 50 dimensional causes that pools the states related to all the 4 patches.

Figure 2 shows the visualization of the receptive fields at each layer. We observe that each dimension of causes in the first layer represents a group of primitive features (like inclined lines) which are localized in orientation or position⁴. Whereas, the causes in the second layer represent more complex features, like corners, angles, etc. These filters are consistent with the previously proposed methods like Lee et al. [5] and Zeiler et al. [7].

3.2 Role of top-down information

In this section, we show the role played by the top-down information during inference, particularly in the presence of structured noise. Video sequences consisting of objects of three different shapes (Refer to Figure 3) were constructed. The objective is to classify each frame as coming from one of the three different classes. For this, several 32×32 pixel 100 frame long sequences were made using two objects of the same shape bouncing off each other and the “walls”. Several such sequences were then concatenated to form a 30,000 long sequence. We train a two layer network using this sequence. First, we divided each frame into 12×12 patches with neighboring patches overlapping by 4 pixels; each frame is divided into 16 patches. The bottom layer was trained such the 12×12 patches were used as inputs and were encoded using a 100 dimensional state vector. A 4 contiguous neighboring patches were pooled to infer the causes that have 40 dimensions. The second layer was trained with 4 first layer causes as inputs, which were itself inferred from 20×20 contiguous overlapping blocks of the video frames. The states here are 60 dimensional long and the causes have only 3 dimensions. It is important to note here that the receptive field of the second layer causes encompasses the entire frame.

We test the performance of the DPCN in two conditions. The first case is with 300 frames of clean video, with 100 frames per shape, constructed as described above. In the second case, we corrupt the video with “structured” noise, where we randomly pick a number of objects from same three shapes with a Poisson distribution (with mean 1.5) and add them to each frame independently at a random locations. There is no correlation between any two consecutive frames regarding where the “noisy objects” are added (see Figure.3b).

First we consider the clean video and perform inference with only bottom-up inference, i.e., during inference we consider $\hat{\mathbf{u}}_t^{(l)} = 0, \forall l \in \{1, 2\}$. Figure 4a shows the scatter plot of the three dimensional causes at the top layer. Clearly, there are 3 clusters recognizing three different shape in the video sequence. Figure 4b shows the same scatter plot when the same procedure is applied on the noisy video. We observe that 3 shapes here can not be clearly distinguished. Finally, we use top-down information along with the bottom-up inference as described in section 2.4 on the noisy data.

⁴Please refer to supplementary material for more results.

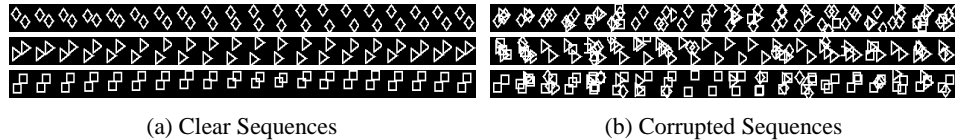


Figure 3: Shows part of the (a) clean and (b) corrupted video sequences constructed using three different shapes. Each row indicates one sequence.

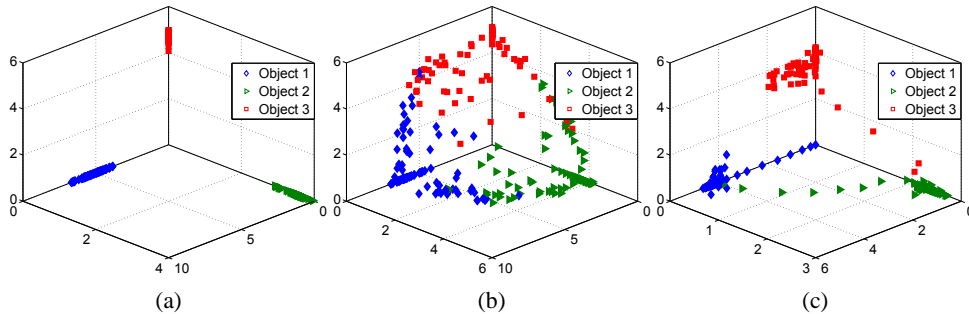


Figure 4: Shows the scatter plot of the 3 dimensional causes at the top-layer for (a) clean video with only bottom-up inference, (b) corrupted video with only bottom-up inference and (c) corrupted video with top-down flow along with bottom-up inference. At each point, the shape of the marker indicates the true shape of the object in the frame.

We argue that, since the second layer learned class specific information, the top-down information can help the bottom layer units to disambiguate the noisy objects from the true objects. Figure 4c shows the same scatter plot for this case. Clearly, with the top-down information, in spite of largely corrupted sequence, the DPCN is able to separate the frames belonging to the three shapes (the trace from one cluster to the other is because of the gradual change from one sequence to the other).

4 Conclusion

In this paper we proposed the deep predictive coding network, a generative model that empirically alters the priors in a dynamic and context sensitive manner. This model composes to two main components: (a) linear dynamical models with sparse states used for feature extraction, and (b) top-down information to adapt the empirical priors. The dynamic model captures the temporal dependencies and reduces the instability usually associated with sparse coding⁵. Whereas, the task specific information from the top layers helps to resolve ambiguities in the lower-layer improving data representation in the presence of noise. We believe that our approach can be extended with convolutional methods, paving the way for implementation of high-level tasks like object recognition, etc., on large scale videos or images.

Acknowledgments

This work is supported by the Office of Naval Research (ONR) grant #N000141010375. We thank Austin J. Brockmeier and Matthew Emigh for their comments and suggestions.

References

- [1] David G. Lowe. Object recognition from local scale-invariant features. In *Proceedings of the International Conference on Computer Vision-Volume 2 - Volume 2, ICCV '99*, pages 1150–, 1999. ISBN 0-7695-0164-8.
- [2] Navneet Dalal and Bill Triggs. Histograms of oriented gradients for human detection. In *Proceedings of the 2005 IEEE Computer Society Conference on Computer Vision and Pattern*

⁵Please refer to the supplementary material for more details.

- Recognition (CVPR'05) - Volume 1 - Volume 01*, CVPR '05, pages 886–893, 2005. ISBN 0-7695-2372-2.
- [3] B. A. Olshausen and D. J. Field. Emergence of simple-cell receptive field properties by learning a sparse code for natural images. *Nature*, 381(6583):607–609, June 1996. ISSN 0028-0836.
 - [4] L. Wiskott and T.J. Sejnowski. Slow feature analysis: Unsupervised learning of invariances. *Neural computation*, 14(4):715–770, 2002.
 - [5] Honglak Lee, Roger Grosse, Rajesh Ranganath, and Andrew Y. Ng. Convolutional deep belief networks for scalable unsupervised learning of hierarchical representations. In *Proceedings of the 26th Annual International Conference on Machine Learning*, ICML '09, pages 609–616, 2009. ISBN 978-1-60558-516-1.
 - [6] K. Kavukcuoglu, P. Sermanet, Y.L. Boureau, K. Gregor, M. Mathieu, and Y. LeCun. Learning convolutional feature hierarchies for visual recognition. *Advances in Neural Information Processing Systems*, pages 1090–1098, 2010.
 - [7] M.D. Zeiler, D. Krishnan, G.W. Taylor, and R. Fergus. Deconvolutional networks. In *Computer Vision and Pattern Recognition (CVPR), 2010 IEEE Conference on*, pages 2528–2535. IEEE, 2010.
 - [8] P. Vincent, H. Larochelle, I. Lajoie, Y. Bengio, and P.A. Manzagol. Stacked denoising autoencoders: Learning useful representations in a deep network with a local denoising criterion. *The Journal of Machine Learning Research*, 11:3371–3408, 2010.
 - [9] Rajesh P. N. Rao and Dana H. Ballard. Dynamic model of visual recognition predicts neural response properties in the visual cortex. *Neural Computation*, 9:721–763, 1997.
 - [10] Karl Friston. Hierarchical models in the brain. *PLoS Comput Biol*, 4(11):e1000211, 11 2008.
 - [11] Geoffrey E. Hinton, Simon Osindero, and Yee-Whye Teh. A Fast Learning Algorithm for Deep Belief Nets. *Neural Comp.*, (7):1527–1554, July .
 - [12] Yoshua Bengio, Pascal Lamblin, Dan Popovici, and Hugo Larochelle. Greedy layer-wise training of deep networks. In *In NIPS*, 2007.
 - [13] Koray Kavukcuoglu, Marc' Aurelio Ranzato, and Yann LeCun. Fast inference in sparse coding algorithms with applications to object recognition. *CoRR*, abs/1010.3467, 2010.
 - [14] Yan Karklin and Michael S. Lewicki. A hierarchical bayesian model for learning nonlinear statistical regularities in nonstationary natural signals. *Neural Computation*, 17:397–423, 2005.
 - [15] H. Zou and T. Hastie. Regularization and variable selection via the elastic net. *Journal of the Royal Statistical Society: Series B (Statistical Methodology)*, 67(2):301–320, 2005.
 - [16] D. Angelosante, G.B. Giannakis, and E. Grossi. Compressed sensing of time-varying signals. In *Digital Signal Processing, 2009 16th International Conference on*, pages 1 –8, july 2009.
 - [17] A. Charles, M.S. Asif, J. Romberg, and C. Rozell. Sparsity penalties in dynamical system estimation. In *Information Sciences and Systems (CISS), 2011 45th Annual Conference on*, pages 1 –6, march 2011.
 - [18] D. Sejdinovic, C. Andrieu, and R. Piechocki. Bayesian sequential compressed sensing in sparse dynamical systems. In *Communication, Control, and Computing (Allerton), 2010 48th Annual Allerton Conference on*, pages 1730 –1736, 29 2010-oct. 1 2010. doi: 10.1109/ALLERTON.2010.5707125.
 - [19] X. Chen, Q. Lin, S. Kim, J.G. Carbonell, and E.P. Xing. Smoothing proximal gradient method for general structured sparse regression. *The Annals of Applied Statistics*, 6(2):719–752, 2012.
 - [20] Amir Beck and Marc Teboulle. A Fast Iterative Shrinkage-Thresholding Algorithm for Linear Inverse Problems. *SIAM Journal on Imaging Sciences*, (1):183–202, March . ISSN 19364954. doi: 10.1137/080716542.
 - [21] Y. Nesterov. Smooth minimization of non-smooth functions. *Mathematical Programming*, 103(1):127–152, 2005.
 - [22] Karol Gregor and Yann LeCun. Efficient Learning of Sparse Invariant Representations. *CoRR*, abs/1105.5307, 2011.
 - [23] Alex Nelson. *Nonlinear estimation and modeling of noisy time-series by dual Kalman filtering methods*. PhD thesis, 2000.

A Supplementary material for Deep Predictive Coding Networks

A.1 From section 2.3.1, computing α^*

The optimal solution of α in (6) is given by

$$\begin{aligned}
 \alpha^* &= \arg \max_{\|\alpha\|_\infty \leq 1} [\alpha^T \mathbf{e}_t - \frac{\mu}{2} \|\alpha\|^2] \\
 &= \arg \min_{\|\alpha\|_\infty \leq 1} \left\| \alpha - \frac{\mathbf{e}_t}{\mu} \right\|^2 \\
 &= S\left(\frac{\mathbf{e}_t}{\mu}\right)
 \end{aligned} \tag{14}$$

where $S(\cdot)$ is a function projecting $\left(\frac{\mathbf{e}_t}{\mu}\right)$ onto an ℓ_∞ -ball. This is of the form:

$$S(x) = \begin{cases} x, & -1 \leq x \leq 1 \\ 1, & x > 1 \\ -1, & x < -1 \end{cases}$$

A.2 Algorithm for joint inference of the states and the causes.

Algorithm 1 Updating $\mathbf{x}_t, \mathbf{u}_t$ simultaneously using FISTA-like procedure [20].

Require: Take $L_{0,n}^x > 0 \forall n \in \{1, 2, \dots, N\}$, $L_0^u > 0$ and some $\eta > 1$.

- 1: Initialize $\mathbf{x}_{0,n} \in \mathbb{R}^K \forall n \in \{1, 2, \dots, N\}$, $\mathbf{u}_0 \in \mathbb{R}^D$ and set $\xi_1 = \mathbf{u}_0$, $\mathbf{z}_{1,n} = \mathbf{x}_{0,n}$.
 - 2: Set step-size parameters: $\tau_{1,n} = 1$ (for states) and $s_1 = 1$ (for causes),
 - 3: **while** no convergence **do**
 - 4: Update $\lambda = (1 + \exp(-[\mathbf{B}\mathbf{u}_k]))/2$.
 - 5: **for** $n \in \{1, 2, \dots, N\}$ **do**
 - 6: **Line search:** Find the best step size $L_{k,n}^x$.
 - 7: Compute α^* from (14)
 - 8: Update $\mathbf{x}_{i,n}$ using the gradient from (9) with a soft-thresholding function.
 - 9: Update internal variables z_{i+1} and τ_{i+1} as in [20].
 - 10: **end for**
 - 11: Compute $\sum_{n=1}^N \|\mathbf{x}_{i,n}\|_1$
 - 12: **Line search:** Find the best step size L_k^u .
 - 13: Update $\mathbf{u}_{i,n}$ using the gradient of (5) with a soft-thresholding function.
 - 14: Update internal variables ξ_{i+1} and s_{i+1} as in [20].
 - 15: Check for convergence.
 - 16: $i = i + 1$
 - 17: **end while return** $\mathbf{x}_{i,n} \forall n \in \{1, 2, \dots, N\}$ and \mathbf{u}_i
-

A.3 Inferring sparse states with known parameters

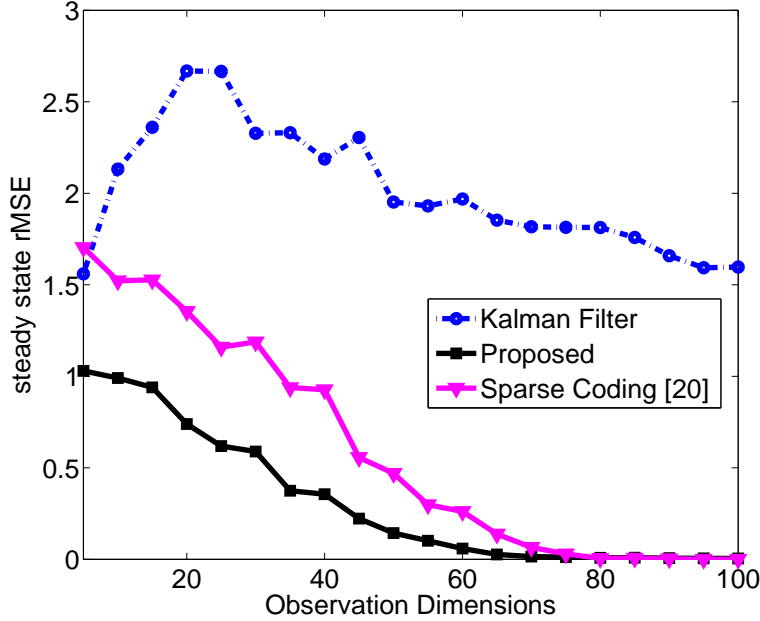


Figure 5: Shows the performance of the inference algorithm with fixed parameters when compared with sparse coding and Kalman filtering. For this we first simulate a state sequence with only 20 non-zero elements in a 500-dimensional state vector evolving with a permutation matrix, which is different for every time instant, followed by a scaling matrix to generate a sequence of observations. We consider that both the permutation and the scaling matrices are known *a priori*. The observation noise is Gaussian zero mean and variance $\sigma^2 = 0.01$. We consider sparse state-transition noise, which is simulated by choosing a subset of active elements in the state vector (number of elements is chosen randomly via a Poisson distribution with mean 2) and switching each of them with a randomly chosen element (with uniform probability over the state vector). This resemble a sparse innovation in the states. We use these generated observation sequences as inputs and use the *a priori* know parameters to infer the states from the dynamic model. Figure 5 shows the results obtained, where we compare the inferred states from different methods with the true states in terms of relative mean squared error (rMSE) (defined as $\|\mathbf{x}_t^{est} - \mathbf{x}_t^{true}\| / \|\mathbf{x}_t^{true}\|$). The steady state error (rMSE) after 50 time instances is plotted versus with the dimensionality of the observation sequence. Each point is obtained after averaging over 50 runs. We observe that our model is able to converge to the true solution even for low dimensional observation, when other methods like sparse coding fail. We argue that the temporal dependencies considered in our model is able to drive the solution to the right attractor basin, insulating it from instabilities typically associated with sparse coding [15].

A.4 Visualizing learned model

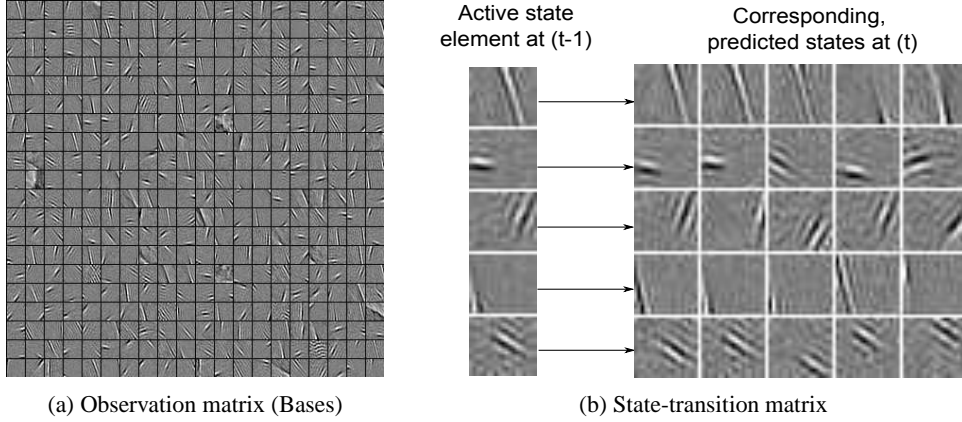


Figure 6: Visualization of the parameters. \mathbf{C} and \mathbf{A} , of the model described in section 3.1. (A) Shows the learned observation matrix \mathbf{C} . Each square block indicates a column of the matrix, reshaped as $\sqrt{p} \times \sqrt{p}$ pixel block. (B) Shows the state transition matrix \mathbf{A} using its connections strength with the observation matrix \mathbf{C} . On the left are the basis corresponding to the single active element in the state at time $(t - 1)$ and on the right are the basis corresponding to the five most “active” elements in the predicted state (ordered in decreasing order of the magnitude).

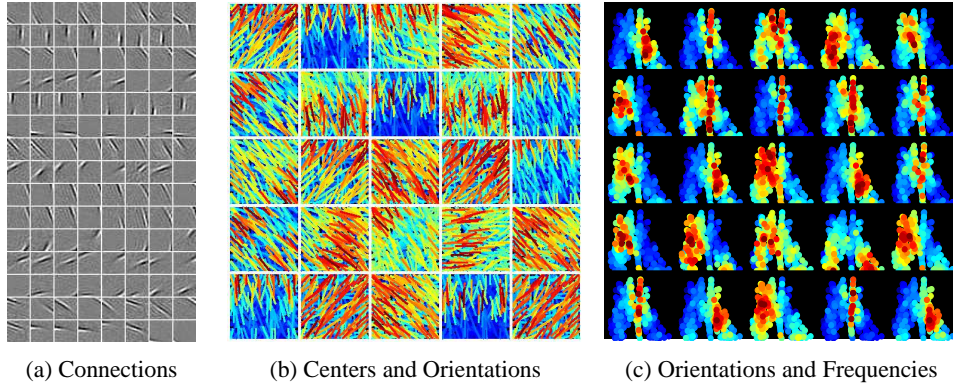


Figure 7: Connections between the invariant units and the basis functions. (A) Shows the connections between the basis and columns of \mathbf{B} . Each row indicates an invariant unit. Here the set of basis that a strongly correlated to an invariant unit are shown, arranged in the decreasing order of the magnitude. (B) Shows spatially localized grouping of the invariant units. Firstly, we fit a Gabor function to each of the basis functions. Each subplot here is then obtained by plotting a line indicating the center and the orientation of the Gabor function. The colors indicate the connections strength with an invariant unit; red indicating stronger connections and blue indicate almost zero strength. We randomly select a subset of 25 invariant units here. We observe that the invariant unit group the basis that are local in spatial centers and orientations. (C) Similarly, we show the corresponding orientation and spatial frequency selectivity of the invariant units. Here each plot indicates the orientation and frequency of each Gabor function color coded according to the connection strengths with the invariant units. Each subplot is a half-polar plot with the orientation plotted along the angle ranging from 0 to π and the distance from the center indicating the frequency. Again, we observe that the invariant units group the basis that have similar orientation.